On the Luminescence of $Ba_5M_4O_{15}$ ($M = Ta^{5+}$, Nb^{5+})

A. M. Srivastava and J. F. Ackerman

G.E. Corporate Research and Development Center, 1 Research Circle, Niskayuna, New York 12309

and

W. W. Beers

G.E. Lighting, Nela Park, Cleveland, Ohio 44112

The low-temperature luminescence properties of the perovskite-derived materials, $Ba_5M_4O_{15}$ ($M = Ta^{5+}$, Nb^{5+}) are reported and discussed. The octahedrally coordinated tantalate groups of $Ba_5Ta_4O_{15}$ exhibit a blue emission, whereas the niobate groups in $Ba_5Nb_4O_{15}$ luminesce yellow upon excitation with short wavelength ultraviolet radiation. The low quenching temperatures of the tantalate and niobate luminescence are a result of energy migration to quenching sites in the host lattice. The luminescence characteristics of $Ba_5Ta_4O_{15}$ and $Ba_5Nb_4O_{15}$ are compared with those reported for other perovskite-based tantalates/niobates and the results are discussed in terms of electronic delocalization of the excited nd^0 configuration.　© 1997 Academic Press

INTRODUCTION

Compounds based on the perovskite structure and containing closed-shell transition metal ions such as Nb^{5+} and Ta^{5+} are of major technological importance for their optoelectronic and ferroelectric properties. Lithium niobate ($LiNbO_3$), the best known example, has been widely studied for its optoelectronic properties (1). The photoluminescence of such materials has also been extensively studied since such properties can potentially interfere with optoelectronic performance (2). Such studies provide us with a rigorous data base suitable for comparing the effect of structural changes on the luminescence properties. This article describes the luminescence properties of the perovskite-type materials, $Ba_5Ta_4O_{15}$ and $Ba_5Nb_4O_{15}$.

Shannon and Katz have determined that $Ba_5(Ta, Nb)_4 O_{15}$ crystallizes with hexagonal symmetry (space group $P3m1$) (3). The structure consists of five close-packed oxygen and barium layers. The Ta^{5+}/Nb^{5+} ions occupy octahedral sites in 4/5 ths. of these layers leaving one pair of close-packed layer per cell devoid of the tantalum/niobium ions.

When viewed in this way the structure appears as strata of (Nb, Ta)–O polyhedra oriented perpendicular to the c axis and separated from each another by regions containing only BaO_{12} polyhedra. Each stratum is four (Nb, Ta)–O octahedral thick with octahedra sharing corners only. In $Ba_5Ta_4O_{15}$, the $Ta^{5+}–O^2–Ta^{5+}$ bond angle within the stratum is close to the ideal 180°.

EXPERIMENTAL

$Ba_5Ta_4O_{15}$ and $Ba_5Nb_4O_{15}$ were synthesized by blending stoichiometric amounts of $BaCO_3$ and Ta_2O_5 (Nb_2O_5) and heating at 1100°C for 10 h. The samples were reground and fired at 1400°C (tantalate) and 1200°C (niobate) for 10 h. X-ray diffraction patterns of the final products indicated single-phase materials. The niobate displays a slight yellow body color, whereas the tantalate has a white body color. Luminescence measurements were performed as described in Ref. (4).

RESULTS AND DISCUSSIONS

The excitation and emission spectra of $Ba_5Ta_4O_{15}$ at 12 K are shown in Fig. 1. The broad emission band exhibits a maximum at 455 mn while the excitation maximum is situated at approximately 265 nm. The Stokes shifts of emission is $\sim 15,760$ cm^{-1}. The excitation and emission transitions are due to charge transfer transitions within the octahedral tantalate groups. The temperature (T_q) at which the luminescence intensity decreases by 50% of the low temperature value is ~ 100 K. Table 1 compares the optical properties of $Ba_5Ta_4O_{15}$ with those of the perovskites $MTaO_3$ ($M = Li^+$, Na^+, K^+) (5) and perovskite-related $Sr_2Ta_2O_7$ (6). The differences and similarities in the optical properties of the tantalates reported in Table 1 may be explained by considering the magnitude of excited state
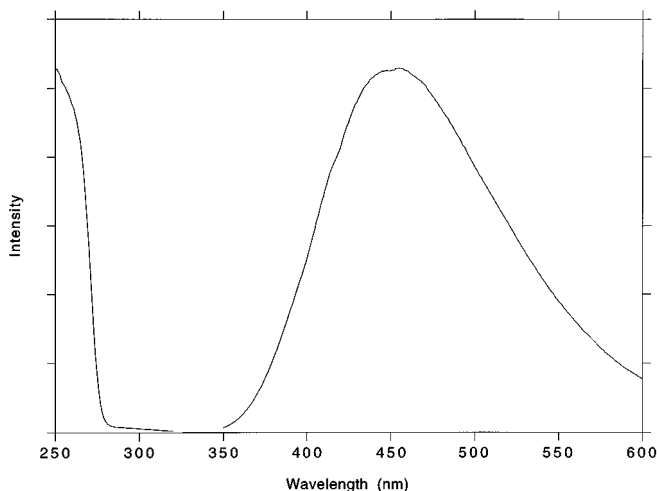
FIG. 1. Excitation ($\lambda_{em} = 455$ nm) and emission ($\lambda_{ex} = 265$ nm) spectra of $Ba_5Ta_4O_{15}$ at $T = 12$ K.

delocalization which is critically dependent on the geometric coupling of the d^0 metal ion polyhedra in the structure. This is discussed below.

Delocalization of the excited state is expected to occur in a structure which offers three-dimensional coupling of the d^0 metal ion polyhedra through corner sharing when the M^{n+}–ligand–M^{n+} bond angle approaches 180° (5). In such cases, the bandwidth (W) of the nd^0 excited state is expected to be quite broad. Deviation of the M^{n+}–ligand–M^{n+} bond angles from 180° causes a reduction in the bandwidth. The eletronic transport properties of solids provide illustrative examples. For example, $LaTiO_3$ with a Ti^{3+}–O^2–Ti^{3+} bond angle of $\sim 157°$ is on the verge of metal–insulator phase boundary, whereas $YTiO_3$ with a bond angle of $\sim 140°$ is a typical Mott insulator with a fairly large charge gap (~ 1 eV) (7).

TABLE 1
Optical Properties of Perovskite–Based Tantalates and Niobates

Compound	Excitation maxima (nm)	Emission maxima (nm)	Stokes shift ($\times 10^3$ cm^{-1})	Reference
$Sr_2Ta_2O_7$	310	485	11.5	(6)
$KTaO_3$	330	490	10.2	(5)
$LiTaO_3$	235	340	14.0	(5)
Ba_3NaTaO_6	245	325	10.0	(8)
$Ba_5Ta_4O_{15}$	265	455	15.5	this work
$LiNbO_3$	260	440	15.7	(5)
$Sr_2Nb_2O_7$	295	475	13.2	(6)
$Ca_2Nb_2O_7$	280	465	14.8	(5)
Ba_3NaNbO_6	280	380	10.0	(8)
$Ba_5Nb_4O_{15}$	305	575	15.5	this work

Thus, when the corner-shared octahedral groups form linear M^{n+}–ligand–M^{n+} linkages the lowest energy absorption/excitation transition is expected to occur at relatively low energy. The emission maxima are generally located at high energies resulting in a small Stokes shift. In contrast, the luminescence of isolated d^0 metal ion polyhedra are usually characterized by a high-energy position of the first absorption band and a large Stokes shift of emission (self-trapped excitonic emission).

We now compare the optical properties of $Ba_5Ta_4O_{15}$ with those reported for other perovskite-derived tantalates in terms of the model discussed above. We first discuss the relative energy position of the first excitation band maxima in $Ba_5Ta_4O_{15}$, $Sr_2Ta_2O_7$, $KTaO_3$, and $LiTaO_3$ (Table 1).

The luminescence of $LiTaO_3$ has been interpreted in terms of isolated tantalate groups in the perovskite lattice (5). The electronic isolation of the tantalate group occurs due to the considerable deviation of the Ta^{5+}–O^2–Ta^{5+} bond angles ($\sim 125°$) from a linear configuration. Since this causes a reduction in W, the first absorption transition occurs at high energy (~ 230 nm). The similarity in the optical properties of $LiTaO_3$ and Ba_3NaTaO_6, with structurally isolated $[TaO_6]^{7-}$ groups is thus not surprising (see Table 1) (5, 8).

The excitation maxima of the other tantalates relative to $LiTaO_3$ and Ba_3NaTaO_6 occur at much lower energies. Lower energy position of the excitation maximum in $KTaO_3$ is expected since the crystal structure offers three-dimensional coupling of corner-shared tantalate octahedra in which the Ta^{5+}–O^2–Ta^{5+} bond angles are close to 180°. Since W in this configuration is expected to be large, the excitation maximum is at low energy and the Stokes shift of emission is small (5).

The crystal structure of $Sr_2Ta_2O_7$ indicates infinite coupling of the corner-linked octahedral units (Ta^{5+}–O^2–Ta^{5+} bond angles close to 180°) along one crystallographic direction while such units are only four octahedra thick along the other two crystallographic directions (9). Therefore, $W[Sr_2Ta_2O_7] < W[KTaO_3]$ since the coupling between the corner-shared tantalate octahedral groups in $Sr_2Ta_2O_7$ is restricted relative to the three-dimensional coupling in $KTaO_3$. This explains the higher energy position of the excitation maximum in $Sr_2Ta_2O_7$ (32, 300 cm^{-1}) relative to $KTaO_3$ (30, 300 cm^{-1}).

In $Ba_5Ta_4O_{15}$ the corner-sharing octahedral groups also exhibit Ta^{5+}–O^2–Ta^{5+} bond angles close to 180°. However, in contrast to $Sr_2Ta_2O_7$ these groups are only four octahedra thick along three orthogonal crystallographic directions. As previously discussed, these chains are terminated by the BaO_{12} polyhedra (3). Since the number of (180°) Ta^{5+}–O^2–Ta^{5+} interactions are severely restricted when compared with $KTaO_3$ and $Sr_2Ta_2O_7$, $W[Ba_5Ta_4O_{15}] < W[Sr_2Ta_2O_7] < W[KTaO_3]$. In agreement, the excitation maximum of $Ba_5Ta_4O_{15}$ (37, 700 cm^{-1}) > $Sr_2Ta_2O_7$

$(32, 300\ cm^{-1}) > KTaO_3$ $(30, 300\ cm^{-1})$. We emphasize that discussion of the experimental results are based on the assumption that the most important interaction responsible for the position of the excitation band is the linear $(180°)$ $Ta^{5+}-O^{2-}-Ta^{5+}$ interaction which strongly promotes extended π bond formation. The influence of other structural details such as the magnitude of tantalate octahedral distortions have not been taken into account. This will become clear when the luminescence of $Ba_5Nb_4O_{15}$ is discussed.

The Stokes shift increases in the sequence $KTaO_3$ $(10, 200\ cm^{-1}) < Sr_2Ta_2O_7$ $(11, 500\ cm^{-1}) < Ba_5Ta_4O_{15}$ $(15, 500\ cm^{-1})$. This agrees with the decreasing bandwidth and hence the decreasing probability of electronic delocalization in the excited state along this series. Since the energy of self-trapping decreases in the sequence $Ba_5Ta_4O_{15}$, $Sr_2Ta_2O_7$, and $KTaO_3$, the emission of $Ba_5Ta_4O_{15}$ may be ascribed to self-trapped exciton recombination as a result of large relaxation in the excited state.

To determine the reason for the low quenching temperature of $Ba_5Ta_4O_{15}$ luminescence the temperature dependence of the $[TaO_6] \rightarrow Eu^{3+}$ energy transfer in $(Ba_{0.98}K_{0.01}E_{0.01})_5Ta_4O_{15}$ was investigated. If the low quenching temperature is due to energy transfer from the $[TaO_6]$ groups to lattice quenching sites then the decrease in the $[TaO_6]$ luminescence intensity with increasing temperature should be accompanied with an increase in the Eu^{3+} intensity provided that the transfer to the intentionally incorporated activator ions (Eu^{3+}) is more efficient than the transfer to the nonradiative quenching sites in the host lattice.

The luminescence of $(Ba_{0.98}K_{0.01}Eu_{0.01})_5Ta_4O_{15}$ at three different temperatures for $\lambda_{ex} = 265$ nm is shown in Fig. 2. The variation with increasing temperature of the integrated luminescence intensity from the $[TaO_6]$ group and from the Eu^{3+} traps is shown in Fig. 3. There is little change in the intensities upto 30 K. Above 30 K, however, the decrease in the $[TaO_6]$ emission intensity is accompanied by an increase in the Eu^{3+} emission intensity. This suggests that the Eu^{3+} ions act as efficient acceptors for the $[TaO_6]$ excitation energy that becomes mobile for $T > 30$ K. The temperature-dependent luminescence quenching of pure $Ba_5Ta_4O_{15}$ is thus attributed to migration of the $[TaO_6]$ excitation energy to nonradiative quenching centers (defect centers) in the host lattice.

The site symmetry around the Eu^{3+} ion can be determined from its luminescence spectrum. The Ba^{2+} ions in $Ba_5Ta_4O_{15}$ are distributed on two different sites with site
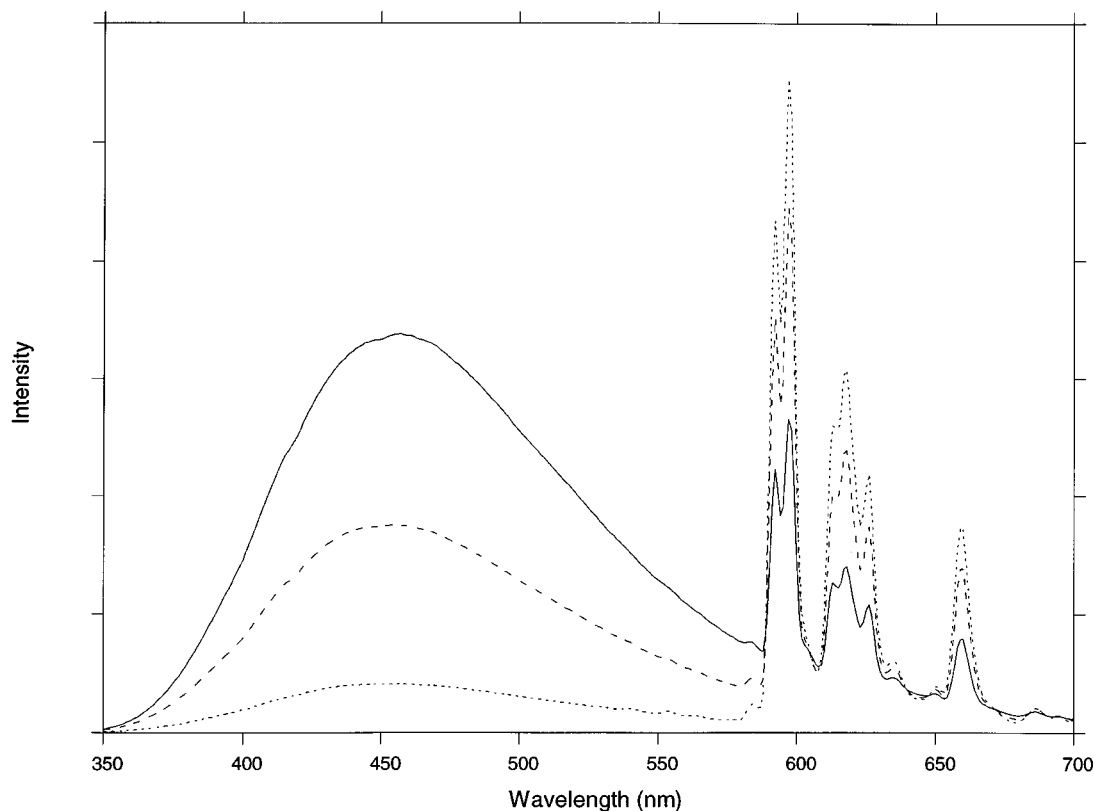

FIG. 2. Emission spectra of $(Ba_{0.98}K_{0.01}Eu_{0.01})_5Ta_4O_{15}$ at $T = 12$ K (solid line), $T = 100$ K (dashed line), and $T = 140$ K (dotted line). Excitation wavelength is 265 nm.

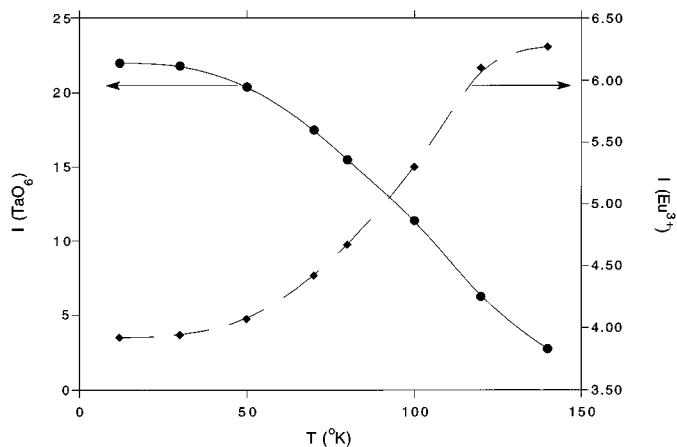**FIG. 3.** Temperature dependence of the integrated $[TaO_6]$ and Eu^{3+} emission intensities in $(Ba_{0.98}K_{0.01}Eu_{0.01})_5Ta_4O_{15}$.

FIG. 4. Excitation ($\lambda_{em} = 580$ nm) and emission ($\lambda_{ex} = 305$ nm) spectra of $Ba_5Nb_4O_{15}$ at $T = 12$ K.

symmetries of C_{3v} and D_{3d}, respectively. The presence of an inversion center allows only the magnetic dipole ($^5D_0 \rightarrow {}^7F_1$) transitions to occur for Eu^{3+} ions in the crystallographic site with D_{3d} symmetry.

Consistent with the Eu^{3+} ions on the site with C_{3v} symmetry is the presence of a single very weak $^5D_0 \rightarrow {}^7F_0$ emission transition at 583 nm (17, 153 cm^{-1}). Note that this transition is forbidden in the D_{3d} symmetry. The higher intensity of the magnetic dipole transitions (0–1) reflects a higher contribution from the Eu^{3+} ions of the D_{3d} site. The Eu^{3+} ions occupying the C_{3v} site are expected to display three lines for the $^5D_0 \rightarrow {}^7F_2$ transitions. Under higher resolution, at least five lines can be distinguished in the emission spectrum. This may reflect deviations from the ideal site symmetry as prescribed by the crystal structure due to the influence of charge compensation which may lower the Eu^{3+} symmetry. This was not investigated further.

The optical properties of $Ba_5Nb_4O_{15}$ (11) were also investigated. The room temperature diffuse reflectance of this material places the absorption edge of ~ 310 nm ($\sim 33,000$ cm^{-1}). The tantalate ($Ba_5Ta_4O_{15}$) absorption edge thus occurs at ~ 5000 cm^{-1} higher energy than the niobate ($Ba_5Nb_4O_{15}$). This observation also suggests a reduced band width of the nd^0 excited state in these materials since the distinction between the optical properties of niobates and tantalates tends to disappear with the dominance of band formation (5). Otherwise, the excitation and emission maxima of the tantalates are always at energies higher than those of the corresponding niobates due to the higher fifth ionization potential of tantalum as compared to niobium (12). The latter condition is clearly applicable in the $Ba_5M_4O_{15}$ ($M = Nb^{5+}, Ta^{5+}$) materials.

The excitation and emission spectra at 12 K are shown in Fig. 4. The excitation maximum at ~ 305 nm is in agree-

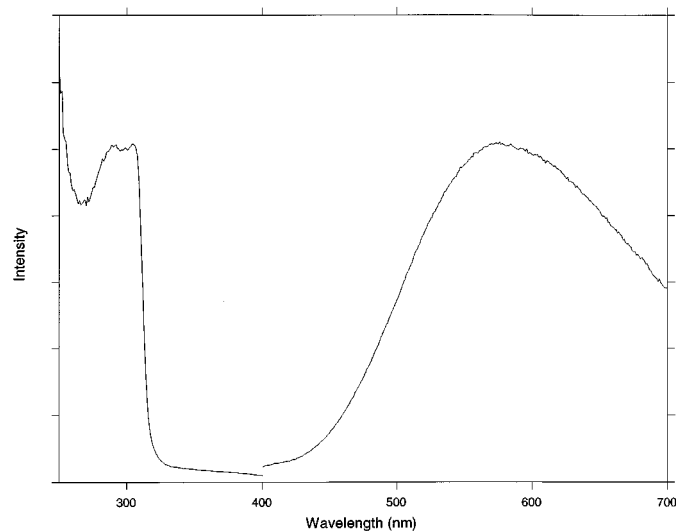ment with the optical absorption edge as determined from the room temperature diffuse reflectance spectrum. The emission consists of a broad band with maximum at ~ 580 nm. The Stokes shift of $\sim 15,500$ cm^{-1} and the quenching temperature of 100 K are comparable to the corresponding tantalate. However, in contrast to $Ba_5Ta_4O_{15}$, the luminescence efficiency of the niobate at $T = 12$ K is very low. The niobate displays a slight yellow body color which deepens with an increase in the synthesis temperature. The luminescence efficiency is also substantially lower in samples synthesized at higher temperatures. The diffuse reflectance spectrum also shows a long tail in the visible region. This indicates a higher concentration of lattice defects or impurity centers in the niobate as opposed to the tantalate. Hence, the low efficiency of $Ba_5Ta_4O_{15}$ is attributed to the higher defect concentration that act as efficient killer sites for the niobate luminescence. The nature of the defect sites is not known.

We note from Table 1 that the excitation band maxima of $Sr_2Nb_2O_7$ and $Ba_5Nb_4O_{15}$ practically coincide. This was unexpected since for the corresponding tantalates it was proposed that $W[Ba_5Ta_4O_{15}] < W[Sr_2Ta_2O_7]$. Hence, we would have expected the excitation maximum of $Ba_5Nb_4O_{15}$ to be at a higher energy relative to $Sr_2Nb_2O_7$ since the number of 180° $Nb^{5+}-O^{2-}-Nb^{5+}$ interactions in the former material is severely restricted. This suggests that in $Ba_5Nb_4O_{15}$ other structural details such as distortions of the octahedral groups is probably playing an important role. The crystal structure of $Sr_2Nb_2O_7$ indicates distorted niobate octahedral groups (13). We propose that the corner-linked niobate octahedral groups are more symmetrical in $Ba_5Nb_4O_{15}$ than in $Sr_2Nb_2O_7$, so that excited state delocalization is more effective in the former material. The

octahedral distortions are then large enough in $Sr_2Nb_2O_7$ to restrict excited state delocalization along the crystallographic axis that contains the infinite corner-linked niobate octahedral groups. Note, however, the lower energy of the excitation maximum in $Ba_5Nb_4O_{15}$ relative to $LiNbO_3$ and Ba_3NaNbO_6. This is expected in view of the discussion presented earlier. A complete structural analysis of $Ba_5Nb_4O_{15}$ is clearly desirable for further comparison.

CONCLUSION

We have studied the luminescence properties of the perovskite–derived $Ba_5M_4O_{15}$ ($M = Nb^{5+}$, Ta^{5+}) material. It is shown through crystal structural considerations that relative to $KTaO_3$ and $Sr_2Ta_2O_7$ the electronic delocalization of excitation energy via band formation is restricted in $Ba_5Ta_4O_{15}$. The luminescence of $Ba_5(Ta, Nb)_4O_{15}$ is ascribed to self-trapped excitonic emission as a result of large relaxation in the excited state and the low quenching temperature of luminescence is due to energy migration to quenching sites in the host lattice.

REFERENCES

1. J. Garcia Sole, B. Macalik, L. E. Bausa, F. Cusso, E. Camarillo, A. Lorenzo, L. Nunez, F. Jaque, A. Monteil, G. Boulon, J. E. Munoz Santiuste, and I. Vergara, *J. Electrochem. Soc.* **140,** 2010 (1993). [and references therein]
2. G. Blasse, *Struct. Bonding* **42,** 1 (1980).
3. J. Shannon and L. Katz, *Acta Cryst. B* **26,** 102 (1970).
4. A. M. Srivastava and W. W. Beers, *J. Electrochem. Soc.* **143,** L203 (1996).
5. G. Blasse and L. G. De Haart, *J. Mater. Chem. Phys.* **14,** 481 (1986); M. Weigel, M. H. J. Emond, E. R. Stobbe, and G. Blasse, *J. Phys. Chem. Solids* **55,** 773 (1994).
6. G. Blasse and L. H. Brixner, *Mater. Res. Bull.* **24,** 363 (1989).
7. D. A. MacLean, Hok-Nam Ng, and J. E. Greedan, *J. Solid State Chem.* **30,** 35 (1979).
8. G. Blasse, G. J. Dirkesn, Pei Zhiwu, G. Wehrum, and R. Hoppe, *Chem. Phys. Lett.* **215,** 363 (1993).
9. N. Ishizawa, F. Marumo, T. Kawamura, and M. Kimura, *Acta Cryst. B* **32,** 2564 (1976).
10. A. M. Srivastava and J. F. Ackerman, *Chem. Mater.* **4,** 1011 (1992). [and references therein]
11. N. E. Massa, S. Pagola, and R. Carbonio, *Phys. Rev.* **53,** 8148 (1996).
12. A. M. Srivastava and J. F. Ackerman, *Mater. Res. Bull.* **26,** 144 (1991). [and references therein]
13. N. Ishizawa, F. Marumo, T. Kawamura, and M. Kimura, *Acta Cryst. B* **31,** 1912 (1975).